Evolution of accretion disks around massive black holes: constraints from the demography of active galactic nuclei

Qingjuan Yu[1,2], Youjun Lu[2] and Guinevere Kauffmann[3]

[2] *Department of Astronomy and Theoretical Astrophysics Center, University of California at Berkeley, Berkeley, CA 94720; yqj@astro.berkeley.edu; lyj@astro.berkeley.edu*

[3] *Max-Planck-Institut für Astrophysik, D-85748 Garching, Germany; gamk@mpa-garching.mpg.de*

ABSTRACT

Observations have shown that the Eddington ratios (the ratio of the bolometric luminosity to the Eddington luminosity) in QSOs/active galactic nuclei (AGNs) cover a wide range. In this paper we connect the demography of AGNs obtained by the Sloan Digital Sky Survey with the accretion physics around massive black holes and propose that the diversity in the Eddington ratios is a natural result of the long-term evolution of accretion disks in AGNs. The observed accretion rate distribution of AGNs in the nearby universe is consistent with the predictions of simple theoretical models in which the accretion rates evolve in a self-similar way. We also discuss the implications of the results for the issues related to self-gravitating disks, coevolution of galaxies and QSOs/AGNs, and the unification picture of AGNs.

Subject headings: black hole physics — accretion, accretion disks — galaxies: active — galaxies: evolution

1. Introduction

The past decade has seen great progress on measuring the mass of massive black holes (BHs) in both nearby normal galaxies and AGNs/QSOs (e.g., Richstone et al. 1998; Wandel et al. 1999; Kaspi et al. 2000). With reliably measured BH masses in AGNs/QSOs, their Eddington ratios (i.e., the ratio of the bolometric luminosity to the Eddington luminosity) can be estimated. Compared to the bolometric luminosity (or the accretion rate, given the mass-to-energy conversion efficiency ϵ), the Eddington ratio (or dimensionless accretion rate) is a normalized parameter and more related to the accretion physics. Observations have shown that the Eddington ratios in AGNs/QSOs cover a wide range (at least 2–3 orders of magnitude) with an upper limit of about 1 (Woo & Urry 2002; McLure & Dunlop 2004). It is natural to ask what determines the diversity of the Eddington ratios. The simplest attempt to answer this question would be by first asking whether the diversity of the Eddington ratios is a consequence of evolution of accretion processes onto BHs.

The questions raised above on the origin of the diversity of the Eddington ratios in AGNs may have important implications for understanding the evolution of the QSO luminosity function (e.g., Schmidt & Green 1983; Boyle et al. 2000). Generally the number density of AGNs/QSOs at a given redshift and luminosity/dimensionless accretion rate should be jointly determined by both the number densities of galaxies whose nuclear activities are triggered at earlier time and the follow-up nuclear luminosity/accretion rate

[1] Hubble Fellow

evolution of individual AGNs/QSOs. The history of the triggering rate is related to the formation and evolution of galaxies (e.g., major mergers of galaxies) and may have a strong cosmic evolution (e.g., Kauffmann & Haehnelt 2000). The follow-up nuclear luminosity/accretion rate evolution of individual AGNs/QSOs is directly related to the evolution of the accretion disk around the BH and the fueling process onto the disk in their host galaxies. In this paper we extract the evolution of the accretion processes from the observational distribution of accretion rates in AGNs. This provides constraints on theoretical models of accretion disk evolution and also illuminates the origin of the diversity of the Eddington ratios.

To extract the information on the nuclear luminosity/accretion rate evolution from observations, statistical methods involving a large sample of AGNs are required since (i) a single AGN may only represent one specific period in a prolonged phase of nuclear activity. A large sample of AGNs with different ages will span all phases of this activity and allow us to extract information about evolution; and (ii) in addition to age, other physical parameters may be important in determining how AGNs evolve and a statistical method may help to clarify these. In § 2, we describe our method of extracting the evolution of accretion processes phenomenologically from the observational distribution of the accretion rates in nearby AGNs (see also the related methods in Yu & Lu 2004a,b). We argue that results for nearby AGNs are not strongly affected by the uncertainty in the nuclear activity triggering history of these objects, because the evolution of the triggering rate at low redshifts ($z < 0.5$) is probably rather weak. Recent progress by the Sloan Digital Sky Survey (SDSS) on the demography of AGNs (http://www.mpa-garching.mpg.de/SDSS/; Kauffmann et al. 2003b; Heckman et al. 2004) makes the application of the method practical. In § 3, we apply the method to a large sample of SDSS AGNs and get the phenomenological constraints on the evolution of accretion processes. We find that the constraints are consistent with theoretical expectations of the accretion disk evolution models shown in § 4. This consistency suggests that the diversity of Eddington ratios in AGNs is probably a natural result of the evolution of the accretion disk around massive BHs. In § 5, we also discuss the implications of the results for the long-term evolution of accretion disks, AGN unification models, and coevolution models of galaxies and QSOs/AGNs etc. Our conclusions are summarized in § 6.

2. Methodology

In this section we analyze how the accretion rate evolution of an AGN is incorporated into the accretion rate distribution of AGNs in the local universe.

Observations have revealed that the central BH mass in nearby normal galaxies is tightly correlated with the velocity dispersion of the bulge components of host galaxies (Ferrarese & Merritt 2000; Gebhardt et al. 2000; Tremaine et al. 2002). We assume that the final BH masses of nearby AGNs after the nuclear activity, M_f, follow the same correlation with velocity dispersion σ, since mass growth of BHs comes mainly from the nuclear activity phase (e.g., Yu & Tremaine 2002; Fabian 2004; Marconi et al. 2004). We describe the correlation through a probability distribution function of $\log M_f$ at a given σ, $P(\log M_f|\sigma)$, and $P(\log M_f|\sigma)d\log M_f$ gives the probability that the logarithm of the BH mass of an AGN with velocity dispersion σ is in the range $\log M_f \rightarrow \log M_f + d\log M_f$. The mean $\log M_f$ at a given σ is denoted by $\langle\log M_f|\sigma\rangle[= 8.13 + 4.02\log(\sigma/200\,\mathrm{km\,s^{-1}})$; Tremaine et al. 2002]. The intrinsic scatter of $P(\log M_f|\sigma)$ around $\langle\log M_f|\sigma\rangle$ is small enough that it is difficult to distinguish from measurement errors, but is less than 0.27 dex (Tremaine et al. 2002). Given the bolometric luminosity of an AGN $L_{\rm bol}$, the mass accretion rate is given by $\dot{M}_{\rm bol} \equiv L_{\rm bol}/(\epsilon c^2)$, where c is the speed of light. In practice, the [OIII] λ5007 line luminosity $L_{\rm [OIII]}$ is often used as a tracer of AGN activity (e.g., see Heckman et al. 2004); and the bolometric luminosity of an AGN may be estimated from its observed [OIII] line luminosity, given its bolometric correction $f_{\rm bol} = L_{\rm bol}/L_{\rm [OIII]}$. We may also define the accretion rate through the [OIII] line luminosity by $\dot{M}_{\rm [OIII]} \equiv f'_{\rm bol}L_{\rm [OIII]}/(\epsilon c^2)$, where $f'_{\rm bol}$ is a factor representing the average bolometric correction between $L_{\rm [OIII]}$ and $L_{\rm bol}$ and given through $\log f'_{\rm bol} = \langle \log f_{\rm bol} \rangle$. The average of the logarithm of the bolometric correction $\langle \log f_{\rm bol} \rangle$ may be obtained by giving the probability distribution function $P(\log L_{\rm [OIII]}|L_{\rm bol})$, which is defined so that $P(\log L_{\rm [OIII]}|L_{\rm bol})dL_{\rm [OIII]}$ is the probability that the logarithm of the [OIII] line luminosity is in the range $\log L_{\rm [OIII]} \rightarrow \log L_{\rm [OIII]} + d\log L_{\rm [OIII]}$ at a given $L_{\rm bol}$. In general, $\dot{M}_{\rm bol}$ and $\dot{M}_{\rm [OIII]}$ are not the same since the bolometric corrections are not the same for all the AGNs.

Given an AGN with nuclear activity triggered at cosmic time t_i and with final BH mass M_f, we describe the evolution of its accretion rate by $\dot{\mathcal{M}}_{\rm bol}(\tau, t_i, M_f)$, where $\tau \equiv t - t_i$ is the physical time passed since the triggering of the nuclear activity. The total time that the AGN will spend with the logarithm of its accretion rate in the range $\log \dot{M}_{\rm bol} \rightarrow \log \dot{M}_{\rm bol} + d\log \dot{M}_{\rm bol}$ at cosmic time $t_l \equiv t(z = z_l) \leq t \leq t(z = 0) \equiv t_0$ is given by (see eq. 15 in Yu & Lu 2004a):

$$\begin{aligned} & T(\dot{M}_{\rm bol}, t_i, M_f)d\log \dot{M}_{\rm bol} \\ \equiv & \sum_k \frac{(\dot{M}_{\rm bol}\ln 10)d\log \dot{M}_{\rm bol}}{\left| d\dot{\mathcal{M}}_{\rm bol}(\tau, t_i, M_f)/d\tau|_{\tau=\tau_k} \right|}, \end{aligned} \tag{1}$$

where τ_k $(k = 1, 2, ...)$ are the solutions of the equation $\dot{\mathcal{M}}_{\rm bol}(M_f, \tau, t_i) = \dot{M}_{\rm bol}$ that satisfy $t_l \leq t_i + \tau_k \leq t_0$, and $T(\dot{M}_{\rm bol}, t_i, M_f) = 0$ if no such solutions exist. In this paper the redshift z_l is set to 0.3 and AGNs with $z \leq z_l$ are taken as nearby AGNs. We define the function $\phi(\dot{M}_{\rm bol}, M_f, \sigma, t)$ so that $\phi(\dot{M}_{\rm bol}, M_f, \sigma, t)d\log \dot{M}_{\rm bol}d\log M_f d\log\sigma$ gives the comoving number density of AGNs at redshift $z(t)$ with the logarithms of the accretion rate, the final BH mass, and the velocity dispersion in the ranges $\log \dot{M}_{\rm bol} \rightarrow \log \dot{M}_{\rm bol} + d\log \dot{M}_{\rm bol}$, $\log M_f \rightarrow \log M_f + d\log M_f$, and $\log\sigma \rightarrow \log\sigma + d\log\sigma$. Given the evolution of the nuclear activity triggering rate $N(t_i, M_f, \sigma)$, which is defined so that $N(t_i, M_f, \sigma)dt_i d\log M_f d\log\sigma$ is the comoving number density of BHs with host galaxy nuclear activity triggered at cosmic time $t_i \rightarrow t_i + dt_i$ and with the logarithms of its final BH mass and velocity dispersion in the ranges $\log M_f \rightarrow \log M_f + d\log M_f$ and $\log\sigma \rightarrow \log\sigma + d\log\sigma$, we have the time integral of $\phi(\dot{M}_{\rm bol}, M_f, \sigma, t)$ given by (cf., eq. 10 in Yu & Lu 2004a)

$$\begin{aligned} & \int_{t_l}^{t_0} \phi(\dot{M}_{\rm bol}, M_f, \sigma, t)dt \\ = & \int_0^{t_0} N(t_i, M_f, \sigma)T(\dot{M}_{\rm bol}, t_i, M_f)dt_i \\ = & \mathbb{N}(\dot{M}_{\rm bol}, M_f, \sigma)\mathbb{T}(\dot{M}_{\rm bol}, M_f), \end{aligned} \tag{2}$$

where

$$\mathbb{N}(\dot{M}_{\rm bol}, M_f, \sigma) \equiv \frac{\int_0^{t_0} N(t_i, M_f, \sigma)T(\dot{M}_{\rm bol}, t_i, M_f)dt_i}{\int_0^{t_0} T(\dot{M}_{\rm bol}, t_i, M_f)dt_i}, \tag{3}$$

and

$$\begin{aligned} \mathbb{T}(\dot{M}_{\rm bol}, M_f) & \equiv \int_0^{t_0} T(\dot{M}_{\rm bol}, t_i, M_f)dt_i, \\ & = \sum_k \int_{\min\{0, t_l - \tau_k\}}^{t_0 - \tau_k} \frac{\dot{M}_{\rm bol}\ln 10}{\left| d\dot{\mathcal{M}}_{\rm bol}(\tau, t_i, M_f)/d\tau|_{\tau=\tau_k} \right|} dt_i \end{aligned} \tag{4}$$

By multiplying equation (2) by $P(\log L_{[\rm OIII]}|L_{\rm bol})$ and then integrating it over $\log \dot{M}_{\rm bol}$ and $\log M_f$, we have

$$\begin{aligned} & \int_{t_l}^{t_0} \Phi(\dot{m}_{[\rm OIII]}, \sigma, t) dt \\ = & \int d\log M_f \int d\log \dot{M}_{\rm bol} P(\log L_{[\rm OIII]}|L_{\rm bol}) \mathbb{N}(\dot{M}_{\rm bol}, M_f, \sigma) \mathbb{T}(\dot{M}_{\rm bol}, M_f), \end{aligned} \tag{5}$$

where

$$\Phi(\dot{m}_{[\rm OIII]}, \sigma, t) = \int d\log M_f \int d\log \dot{M}_{\rm bol} P(\log L_{[\rm OIII]}|L_{\rm bol}) \phi(\dot{M}_{\rm bol}, M_f, \sigma, t), \tag{6}$$

$\dot{m}_{[\rm OIII]} \equiv \dot{M}_{[\rm OIII]}/\dot{M}_{\rm Edd}[M'_f(\sigma)]$ is the normalized accretion rate, $M'_f(\sigma) = 10^{\langle \log M_f|\sigma \rangle}$, $\dot{M}_{\rm Edd}[M'_f(\sigma)] \equiv L_{\rm Edd}[M'_f(\sigma)]/(\epsilon c^2)$, and $L_{\rm Edd}[M'_f(\sigma)]$ is the Eddington luminosity of a BH with mass $M'_f(\sigma)$. Note that here the definition of the normalized accretion rate is a little different from the conventionally defined Eddington ratio in that $\dot{M}_{[\rm OIII]}$ may not be the same as $\dot{M}_{\rm bol}$, and the Eddington luminosity used here is for the *average final* BH mass, rather than for the BH mass that is powering the nuclear activity in an AGN. If the bolometric correction of each AGN in the sample and its BH mass that is powering the nuclear activity are obtained from future observations, we may construct the methods for the distribution of the Eddington ratios as above and perform a consistency check on the results.

We can further define the time-averaged accretion rate and velocity distribution function of nearby AGNs (with $z \leq z_l$) by

$$\bar{\Phi}(\dot{m}_{[\rm OIII]}, \sigma) \equiv \frac{\int_{t_l}^{t_0} \Phi(\dot{m}_{[\rm OIII]}, \sigma, t) dt}{t_0 - t_l}. \tag{7}$$

Below we assume that the triggering rate of nearby AGNs $N(t_i, M_f, \sigma) = n(t_i, \sigma) P(\log M_f|\sigma)$, where $n(t_i, \sigma) = \int d\log M_f N(t_i, M_f, \sigma)$ is independent of M_f. By further assuming that $n(t_i, \sigma)$ is independent of t_i, we have $\mathbb{N}(\dot{M}_{\rm bol}, M_f, \sigma) = N(t_i, M_f, \sigma)$; and then by combining equations (5) and (7), we have

$$\begin{aligned} & \bar{\Phi}(\dot{m}_{[\rm OIII]}, \sigma) \\ = & \ n(\sigma) \int d\log M_f P(\log M_f|\sigma) \int d\log \dot{M}_{\rm bol} P(\log L_{[\rm OIII]}|L_{\rm bol}) \frac{\mathbb{T}(\dot{M}_{\rm bol}, M_f)}{t_0 - t_l}. \end{aligned} \tag{8}$$

If $\tau_k < t_l$ ($k = 1, 2, ...$; which is satisfied by the assumed models and its best-fit parameters shown in Fig. 2 below) and $\dot{\mathcal{M}}_{\rm bol}(\tau, t_i, M_f)$ does not change with t_i, we have $\mathbb{T}(\dot{M}_{\rm bol}, M_f) \propto t_0 - t_l$ (eq. 4), $\bar{\Phi}(\dot{m}_{[\rm OIII]}, \sigma) = \Phi(\dot{m}_{[\rm OIII]}, \sigma, t)$ at $z(t) \leq z_l$, and $\Phi(\dot{m}_{[\rm OIII]}, \sigma, t)$ is independent of t. In reality AGNs may have a high triggering rate at high redshifts, however, AGNs triggered at high redshifts may have become faint enough at the current epoch to move out of the range of the accretion rates of interest in this paper. For example, using the accretion rate evolution model assumed below (eqs. 9 and 10) and the best-fit parameters obtained in § 3, only those AGNs whose nuclear activities are trigerred at $z < 0.5$ may have an accretion rate high enough at $z < z_l$ to be within the range shown in Figure 1 below. As an additional check, we have assumed that the triggering rate is proportional to the major merger rate of galaxies, e.g., $n(t_i, \sigma) \propto [1 + z(t_i)]^\alpha$ with $\alpha = 0.51 \pm 0.28$ (Lin et al. 2004) and our results are not significantly affected.

It is plausible to assume that the growth of a BH involves two phases after the nuclear activity is triggered on (Yu & Lu 2004a; see also Small & Blandford 1992). In the first (or "demand limited") phase, there is plenty of material to fuel BH growth. However, not all of the available material can contribute to the BH growth immediately and the BH growth is limited by the Eddington luminosity. We assume that the BH accretes with the Eddington luminosity for a period τ_I and denote the BH mass at cosmic time $t_I = t_i + \tau_I$ by M_I. We assume the mass-to-energy conversion efficiency ϵ to be a constant. Thus, the accretion rate in the first phase increases with time as follows:

$$\dot{\mathcal{M}}_{\rm bol}(\tau) = \dot{M}_{\rm Edd}(M_I)\exp\left(\frac{\tau-\tau_I}{\tau_{\rm Sp}}\right), \qquad 0<\tau<\tau_I, \tag{9}$$

where $\tau_{\rm Sp} = 4.5 \times 10^7 \epsilon/[0.1(1-\epsilon)]$ yr is the Salpeter time [the time for a BH radiating at the Eddington luminosity to e-fold in mass; we set $\epsilon/(1-\epsilon) = 0.1$ below]. With the decline of material supply, the BH growth enters into the second (or "supply limited") phase and the nuclear luminosity is expected to decline below the Eddington luminosity. Below we assume that the accretion rate in the second phase evolves as follows:

$$\dot{\mathcal{M}}_{\rm bol}(\tau) = \dot{M}_{\rm Edd}(M_I)\left(\frac{\tau-\tau_I+\tau_D}{\tau_D}\right)^{-\gamma}, \qquad \tau \geq \tau_I, \tag{10}$$

where $\dot{\mathcal{M}}_{\rm bol}(\tau) \propto \tau^{-\gamma}$ at $\tau - \tau_I \gg \tau_D$ and τ_D is the characteristic transition timescale from the first phase to the power-law declining stage of the accretion rate. We assume that the two phases appear only once for an AGN. The final BH mass obtained after the nuclear activity is given by

$$\begin{aligned} M_f &= M_I + \int_{t_I}^{\infty}(1-\epsilon)\dot{\mathcal{M}}_{\rm bol}(\tau)dt \\ &= \left[1+\frac{\tau_D}{(\gamma-1)\tau_{\rm Sp}}\right]M_I, \end{aligned} \tag{11}$$

where the efficiency ϵ is assumed to be the same as the efficiency in the first phase. Here we do not consider that the accretion process may transit to a radiatively inefficient mode when the accretion rate becomes low enough (i.e., when the Eddington ratio is < 0.01; Narayan & Yi 1994; Blandford & Begelman 1999). Such rates are in any case below the accretion rate range studied in this paper (see Fig. 1). For simplicity, below we assume that the timescales τ_I and τ_D are independent of M_f.

According to the accretion rate evolution model assumed above and equations (1)–(6), $\bar{\Phi}(\dot{m}_{\rm [OIII]}, \sigma)$ is roughly constant with $\log \dot{m}_{\rm [OIII]}$ if most AGNs are in the first phase and is proportional to $\dot{m}_{\rm [OIII]}^{-1/\gamma}$ if most AGNs are at the late power-law declining stage of the accretion rate. If the scatter of the distributions $P(\log M_f|\sigma)$ is sufficiently small and the bolometric correction $f_{\rm bol}$ is roughly a constant, $\dot{m}_{\rm [OIII]}$ has a maximum given by

$$\dot{m}_{\rm max} \equiv [1 + (\tau_D/\tau_{\rm Sp})/(\gamma-1)]^{-1} \tag{12}$$

when the AGN is transiting from the first phase to the second phase.

3. Application to observations

The SDSS has obtained a large sample of 33,589 narrow-line AGNs in the local universe (http://www.mpa-garching.mpg.de/SDSS/Data/agncatalogue.html). Details of the sample selection and the derivation of the AGN properties used in this paper [$L_{\rm [OIII]}$, σ, μ_* (the stellar surface mass density)] are given in Kauffmann et al. (2003a,b) and Heckman et al. (2004). In this section we fit the accretion rate evolution models assumed in § 2 (eqs. 9 and 10) to these observed AGNs. (Note that Seyfert I AGNs are not included in this sample because for these objects the AGN itself may have a significant impact at least on the estimate of the velocity dispersion. Possible effects on our conclusions if including Seyfert I galaxies will be discussed at the end of this section.)

We consider AGNs with $L_{[\rm OIII]} \geq L_{[\rm OIII],min} = 10^6 L_\odot$, $\sigma \geq \sigma_{\rm min} = 70\,{\rm km\,s^{-1}}$, and $\mu_* > 3 \times 10^8\,{\rm M_\odot\,kpc^{-2}}$. A sample of fainter AGN is incomplete because at larger distances, the fiber samples more of the stellar light of the host galaxy and weak emission lines become difficult to detect. The lower limit on velocity dispersion is set by the instrumental resolution of the SDSS spectrograph. The galaxies with lower stellar surface mass densities are mainly disk-dominated (Kauffmann et al. 2003a), and their velocity dispersions may be substantially affected by the disk components. (Note that the quantity $L_{[\rm OIII]}$ used here is not extinction-corrected. The extinction effect may be implicitly included in the scatter of the bolometric correction used in the calculations below. See more discussions in Heckman et al. 2004). We get the observational distribution $\bar{\Phi}^{j,k}_{\rm obs}(\dot{m}_{[\rm OIII]},\sigma)$ ($j = 1, 2, ..., 6$; $k = 1, 2...$) by counting the AGNs in such bins: (i) the bin of the velocity dispersions is $[\log\sigma_j, \log\sigma_{j+1}]$, where $\log(\sigma_j/\sigma_{\rm min}) = (j-1)\Delta\log\sigma$ and the bin size $\Delta\log\sigma = 0.05\,{\rm dex}$. We have $\sigma_6 \simeq 140\,{\rm km\,s^{-1}}$ and the range of the black hole mass $M'_f(\sigma)$ over the five bins of the velocity dispersion is 2.0×10^6–$3.2 \times 10^7\,{\rm M_\odot}$. We do not consider objects with larger velocity dispersions in this paper mainly for three reasons: (a) these objects generally have relatively low normalized accretion rate, high BH masses and probably long ages, and thus their distribution could be more affected by both the uncertainty in the efficiency ϵ and the cosmic evolution of the nuclear activity triggering history; (b) the low accretion rate in these objects rate (e.g., $\dot{m} \ll 10^{-3}$) may be simply caused by Bondi accretion; and (c) the assumption that τ_D are independent of M_f may be violated for a wide range of M_f. (ii) The bin of the normalized [OIII] line accretion rate is $[\log\dot{m}_{[\rm OIII],k}, \log\dot{m}_{[\rm OIII],k+1}]$, where $\log(\dot{m}_{[\rm OIII],k}/\dot{m}_{[\rm OIII],min}) = (k-1)\Delta\log\dot{m}_{[\rm OIII]}$, $\dot{m}_{[\rm OIII],min} = \log L_{[\rm OIII],min} - \log L_{\rm Edd}(\langle M_f\rangle) + \log f'_{\rm bol}$, and the bin size $\Delta\log\dot{m}_{[\rm OIII]} = \Delta\log\sigma \times d\log[M'_f(\sigma)]/d\log\sigma \simeq 0.20\,{\rm dex}$. Each observed AGN i has a weighted factor $1/V_{{\rm max},i}$, where $V_{{\rm max},i}$ is the volume over which the object would have been detectable (Schmidt 1968). The quantity $\bar{\Phi}^{j,k}_{\rm obs}(\dot{m}_{[\rm OIII]},\sigma)$ is obtained by summing up the weighted factors ($\sum_i 1/V_{{\rm max},i}$) of AGNs in each bin, and its error $\delta\bar{\Phi}^{j,k}_{\rm obs}$ is estimated by $(\sum_i 1/V^2_{{\rm max},i})^{1/2}$ (see crosses and triangles and their dotted error bars in Fig. 1). Note that the realistic error may not be well represented by the estimate above if the number of AGNs in a bin is small. Below in the fit we do not use the points (i.e., open triangles in Fig. 1) with only one AGN in their bins. In each velocity dispersion bin, the falloff of $\bar{\Phi}^{j,k}_{\rm obs}(\dot{m}_{[\rm OIII]},\sigma)$ at the low-accretion-rate end (see crosses in Fig. 1) is caused by the luminosity cut at $L_{[\rm OIII]} = L_{[\rm OIII],min}$ and these crosses are not used in the fit, either.

We estimate the model distribution of $\bar{\Phi}^{j,k}_{\rm mod}(\dot{m}_{[\rm OIII]},\sigma)$ by first using equation (8) to obtain $\bar{\Phi}_{\rm mod}(\dot{m}_{[\rm OIII]},\sigma)$, and then binning the distribution and normalizing it by setting $\sum_k \bar{\Phi}^{j,k}_{\rm mod}(\dot{m}_{[\rm OIII]},\sigma) = \sum_k \bar{\Phi}^{j,k}_{\rm obs}(\dot{m}_{[\rm OIII]},\sigma)$ ($j = 1, 2, ..., 6$), where the sums are taken over the bins with $\bar{\Phi}^{j,k}_{\rm obs}(\dot{m}_{[\rm OIII]},\sigma) \neq 0$ (but excluding the bins of crosses and open triangles shown in Fig. 1; similarly for the sum in χ^2 below). We assume that $P(\log M_f|\sigma)$ follows a Gaussian distribution with an intrinsic scatter of 0.2 dex around $\langle\log M_f|\sigma\rangle$ (the value of the scatter is set with some degree of arbitrariness, since as mentioned in § 2 the intrinsic scatter is difficult to distinguish from measurement errors but is less than 0.27 dex; Tremaine et al. 2002. See also discussions at the end of this paragraph). The distribution of $P(\log L_{[\rm OIII]}|L_{\rm bol})$ is assumed to be independent of $L_{\rm bol}$ and also follow a Gaussian distribution with $\langle\log(1/f_{\rm bol})\rangle = \langle\log(L_{[\rm OIII]}/L_{\rm bol})\rangle \sim \log(1/3500)$ and a scatter of $\sim 0.38\,{\rm dex}$ (Heckman et al. 2004). We use the χ^2 statistic to fit the model distribution to the observational distribution of $\bar{\Phi}^{j,k}_{\rm obs}(\dot{m}_{[\rm OIII]},\sigma)$ ($j = 1, 2, ..., 6$; $k = 1, 2, ...$). The best-fitted parameters are obtained by minimizing $\chi^2 \equiv \Sigma_{k,j}[(\log\bar{\Phi}^{j,k}_{\rm mod} - \log\bar{\Phi}^{j,k}_{\rm obs})/\delta\log\bar{\Phi}^{j,k}_{\rm obs}]^2$. Here the number of degrees of freedom is $n = 41$. We use P_{χ^2} to denote the probability of χ^2 being higher by chance if the data were drawn from the model. Our a priori definition of an acceptable fit is one with $P_{\chi^2} > 0.01$. For different $\tau_I/\tau_{\rm Sp} = 5, 1, 0.1, 0$, we obtain the best fits for parameters $(\gamma, \tau_D/\tau_{\rm Sp})$ (see crosses in Fig. 2), and all of them are acceptable with $P_{\chi^2} \simeq 0.15$–0.20. The contour plots of confidence levels for the best-fit parameters are shown in Figure 2. The obtained best-fit parameters are insensitive to τ_I and the average of the best fits over four cases of $\tau_I/\tau_{\rm Sp}$ is $(\gamma, \tau_D/\tau_{\rm Sp}) \simeq (1.3, 3.7)$. We take the errors of the fit parameters as $\delta\gamma \simeq^{+0.25}_{-0.15}$ and $\delta(\tau_D/\tau_{\rm Sp}) \simeq^{+3}_{-2}$, which roughly correspond to the 68 per cent confidence contours (i.e., $\chi^2 - \chi^2_{\rm min} = 2.30$) shown in Figure 2. The best-fit parameters (γ, τ_D) may be affected by the values of the scatter in the $M_f - \sigma$ relation and the bolometric correction but generally do not exceed the errors above [e.g., if the intrinsic scatter of $P(\log M_f|\sigma)$ is 0.27 dex, the best fits are $(\gamma, \tau_D/\tau_{\rm Sp}) \simeq (1.4, 6.3)$]. Precise understanding of the evolution of accretion processes would require precise measurements of this scatter (see also Yu & Lu 2004a).

In Figure 1, we show the model distribution $\bar{\Phi}^{j,k}_{\rm mod}(\dot{m}_{\rm [OIII]}, \sigma)$ obtained with $(\tau_I/\tau_{\rm Sp}, \gamma, \tau_D/\tau_{\rm Sp}) \simeq (1, 1.3, 3.7)$ as solid lines. In Figure 1, although there exist AGNs with $\log \dot{m}_{\rm [OIII]} > \log \dot{m}_{\rm max} \simeq -1.1$, the existence of these AGNs does not necessarily mean that they are accreting at a super-Eddington rate with $\dot{M}_{\rm bol} > \dot{M}_{\rm Edd}(M_{\rm BH})$ [here $\dot{M}_{\rm Edd}(M_{\rm BH})$ is the conventionally defined Eddington accretion rate for the BH mass $M_{\rm BH}$ that is powering the nuclear activity in the AGN, not the final mass M_f after the nuclear activity]. In the accretion evolution model used here, we always have $\dot{M}_{\rm bol} < \dot{M}_{\rm Edd}(M_{\rm BH})$. The existence of $\dot{m}_{\rm [OIII]} > \dot{m}_{\rm max}$ is caused by the non-zero scatter of the $M_f - \sigma$ relation and the bolometric correction.

The value of $\tau_D/\tau_{\rm Sp} \simeq 3.7^{+3}_{-2}$ above is obtained by using the number distribution of AGNs as a function of accretion rate. Generally, the timescale related to the length of the nuclear activity may also be constrained by comparing the number density ratio of AGNs to their remnants (e.g., Yu & Tremaine 2002). The predicted ratio of the number density of nearby AGNs to nearby inactive galaxies is affected by uncertainties in the triggering history of AGNs at high redshifts and hence does not help us obtain a more precise constraint.

In addition, we have also assumed an exponentially declining form of the accretion rate evolution in the second phase of the accretion model instead of the power-law declining form and found that all fits are unacceptable with $P_{\chi^2} < 10^{-10}$.

As mentioned above, the observational sample used here does not include Seyfert I galaxies. The fraction of Type II AGNs in the SDSS is a weak function of AGN luminosity, decreasing from $\sim 60\%$ to $\sim 30\%$ over the range $L_{\rm [OIII]} \simeq 10^{5.5} - 10^{8.5}\,{\rm L}_\odot$ (Hao et al. 2005; Heckman et al. 2004). Thus, the fraction of AGNs with high accretion rates (e.g., at $\dot{m}_{\rm [OIII]} \sim 10^{-1}$–$1$; see Fig. 2) could be underestimated here, which will mainly affect the estimate of τ_D. After including Type I galaxies, the best-fit parameter τ_D would decrease slightly and γ would increase, resulting in an increase in $\dot{m}_{\rm max}$ (eq. 12). If we assume that the dependence of the fraction of Type II AGNs on accretion rate is the same as the dependence on luminosity, after including Type I AGNs, we find that the distributions (at the high accretion rates) shown in Figure 1 move upwards by at most $\log 2 \simeq 0.3$ dex. The value of $\tau_D/\tau_{\rm Sp}$ would then have to change from 3.7 to 2.5 in order to compensate.

4. Comparison with accretion disk evolution models

The process that removes the angular momentum of gas in a galaxy and drives into the very central region is still not well understood. It may require a hierarchy of mechanisms, handing off to one another as the material moves inward. Here we consider the "last stop" of the "handing-off". We hypothesize that some mechanism has moved gas to the central parsec in the galaxy, where it will then diffuse to the central BH through viscous transport (or specifically by the magneto-rotational instability) in an accretion disk. The surface mass density, Σ, of an accretion disk with a central, dominant gravitating point mass and with

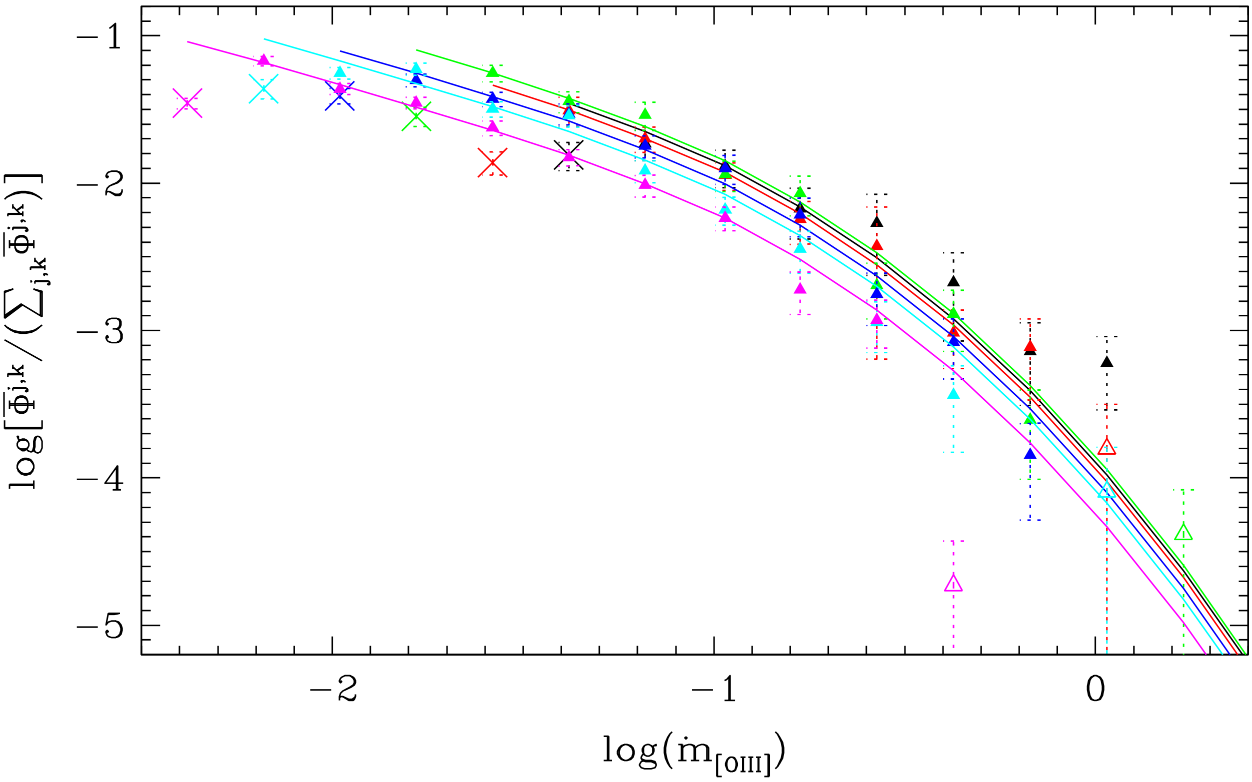

Fig. 1.— The distribution of the normalized accretion rate $\dot{m}_{[\mathrm{OIII}]}$ in nearby AGNs ($z < 0.3$). See the difference between $\dot{m}_{[\mathrm{OIII}]}$ and the conventionally defined Eddington ratio in § 2. Different colors represent different velocity dispersion bins $[\log \sigma_j, \log \sigma_{j+1}]$ (the colors black, red, green, blue, cyan, and magenta correspond to $j = 1, 2, ..., 6$ respectively) with $\sigma_1 = 70\,\mathrm{km\,s^{-1}}$, $\sigma_6 \simeq 140\,\mathrm{km\,s^{-1}}$, and the bin size $\Delta \log \sigma = 0.05$ dex. The observational distribution obtained from nearby Seyfert IIs are drawn as triangles or crosses at the middle point of each $\log(\dot{m}_{[\mathrm{OIII}]})$ bin and their error bars are shown by dotted lines. For open triangles, only one AGN is in each bin. The falloff of crosses at the low-$\dot{m}_{[\mathrm{OIII}]}$ end is caused by the luminosity cut at $L_{[\mathrm{OIII}]} = L_{[\mathrm{OIII}],\mathrm{min}}$. The binned model distributions, obtained with $(\tau_I/\tau_{\mathrm{Sp}}, \gamma, \tau_D/\tau_{\mathrm{Sp}}) = (1, 1.3, 3.7)$, are connected by solid curves (for view clarity, the binned distributions are not drawn in the form of a histogram). See details in § 3.

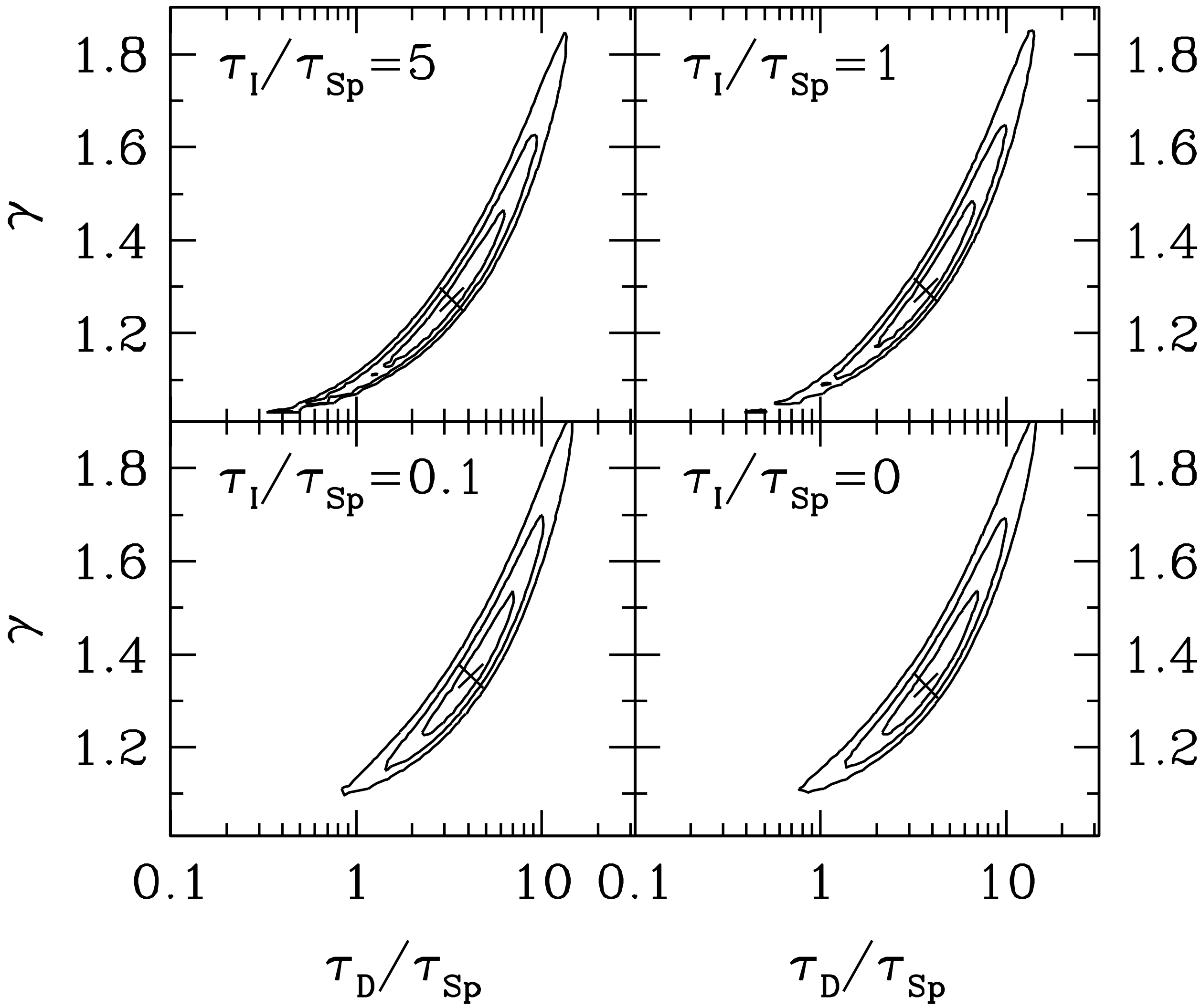

Fig. 2.— Contour of the confidence levels for the best-fitted parameters γ and τ_D. The best-fit parameters are shown by crosses. The contours enclose the 68.3%, 95.4%, and 99.7% confidence regions on them in each panel. See details in § 3.

viscosity ν evolves as a function of time τ and radius R through the equation

$$\frac{\partial \Sigma}{\partial \tau} = \frac{3}{R}\frac{\partial}{\partial R}\left[R^{1/2}\frac{\partial}{\partial R}(\nu \Sigma R^{1/2})\right]. \tag{13}$$

If the viscosity is of the form $\nu(R,\Sigma) \propto R^m \Sigma^n$ (m and n are constants), this equation has solutions of self-similar form (Pringle 1981) as follows:

$$\frac{\Sigma(R,\tau)}{\Sigma_0} = \left(\frac{\tau}{\tau_0}\right)^{\eta} f\left[\left(\frac{R}{R_0}\right)\left(\frac{\tau}{\tau_0}\right)^{\xi}\right], \tag{14}$$

where the values of η and ξ are determined by the exponents m and n in the function $\nu(R,\Sigma)$ and also by the detailed boundary conditions of the accretion disk. Σ_0, R_0, and τ_0 are scale variables with arbitrary dimensions and they satisfy $\tau_0 = R_0^2/\nu(R_0,\Sigma_0)$. The self-similar evolution of accretion disks have also been calculated using numerical simulations (e.g, Lin & Pringle 1987; Cannizzo, Lee & Goodman 1990; Pringle 1991). For an accretion disk with negligible torque at both the origin $R = 0$ and its outer boundary (so that its total angular momentum is conserved during its evolution), the rate at which the mass of the disk decreases is given by a power-law of the form $\dot{M}_d(\tau) = \frac{d}{d\tau}(\int 2\pi\Sigma R dR) \propto \tau^{-\frac{38+18a+4b}{32+17a+2b}}$, where a and b are the exponents in the opacity law $\kappa(\rho,T) = \kappa_0\rho^a T^{-b}$ (e.g., Cannizzo, Lee & Goodman 1990). If $a = b = 0$ (Thomson opacity), we have $\eta = -15/16$, $\xi = -3/8$, $f(x) = (28)^{-3/2}x^{-3/5}(1 - x^{7/5})^{3/2}$ in equation (14), and the mass accretion rate evolves as

$$|\dot{M}_d(\tau)| = \frac{(16/3)M_{d,0}}{\tau_0}\left(\frac{\tau}{\tau_0}\right)^{-19/16}, \tag{15}$$

where $M_{d,0} = (28)^{-3/2}\frac{4\pi}{7}R_0^2\Sigma_0$, and the diffusion timescale of the disk

$$\tau_0 = \frac{R_0^2}{\nu(R_0,\Sigma_0)} = 1.5\times 10^8\,\mathrm{yr}\left(\frac{R_0}{0.5\,\mathrm{pc}}\right)^{7/3}\left(\frac{M_{\rm BH}}{10^7\,\mathrm{M}_\odot}\right)^{1/3} \times\left(\frac{\alpha}{0.1}\right)^{-4/3}\left(\frac{M_{d,0}}{10^7\,\mathrm{M}_\odot}\right)^{-2/3}, \tag{16}$$

where α is the commonly-used parameter related to the viscosity in the standard accretion disk model, and R_0 may be taken as the size of the accretion disk or the location of its reservoir. The reference value of R_0 in equation (16), 0.5 pc, is roughly consistent with the observations on the accretion disks in several nearby AGNs (e.g., NGC4258, Miyoshi et al. 1995; NGC1068, Lodato & Bertin 2003; and NGC 3079, Kondratko et al. 2005). If $a = 1$ and $b = 7/2$ (Kramers opacity), we have $|\dot{M}_d| \propto \tau^{-5/4}$.

Note that the best-fit parameter $\gamma = 1.3^{+0.25}_{-0.15}$ is generally consistent with the exponent (-1.18 or -1.25) of τ in $\dot{M}_d$ expected from the self-similar solutions above. The diffusion timescale $\tau_0[\simeq 3\tau_{\rm Sp}(\epsilon = 0.1)]$ in equation (16) is also consistent with τ_D obtained from observations. These consistencies between the observations and the theoretical expectations above are an encouraging result. They support the hypothesis that the observed diversity in the Eddington ratios of AGNs results from an evolutionary sequence of accretion processes. They also suggest that the accretion disks of most Seyfert galaxies are currently in the self-similar phase or are transiting towards this phase.

5. Discussions

Despite the encouraging consistency above, the self-similar solution of the accretion disk evolution shown in § 4 is based on highly simplified accretion disk models. For example, the effects on the disk evolution by disk winds or by infalling material that is continuously deposited onto the disk are not considered. The role of possible disk instabilities is not considered, either. More complete investigations on the long-term evolution of accretion disks are needed.

There are also further issues to be considered:

- *Self-gravitating disks and star formation:* With the best-fit parameters obtained for the accretion evolution in § 3, the disk is self-gravitating in its early evolutionary stage and the central BH mass becomes dominant in its late evolutionary stage. We note that this evolutionary pattern of the disk mass is probably compatible with current observations of the accretion disks in a few AGNs. For example, NGC3079 (Kondratko et al. 2005) and NGC1068 (Lodato & Bertin 2003) have an Eddington ratio close to 1, which may correspond to the first "demand-limited" phase or a transition to the self-similar evolution of the second phase. Their accretion disks appear to be thick with masses larger than or comparable to their central BH masses. NGC4258 has an Eddington ratio $\lesssim 0.01$ (Gammie et al. 1999), so it may be in the late stage of self-similar evolution, and its accretion disk is thin with a mass that is much smaller than its BH mass (Miyoshi et al. 1995). The evolution of a self-gravitating disk may not exactly follow the simple prescription adopted in this paper. Recently, Fromang et al. (2004) simulated the evolution of self-gravitating tori around a massive BH and found that they quickly evolve to a dual structure with an inner thin Keplerian disk fed by an outer thicker self-gravitating disk. Further investigation of the long term evolution of self-gravitating disks is crucial for understanding the transition to the self-similar phase. In addition, in a self-gravitating disk, star formation may be important because of gravitational instabilities that develop in the disk (Goodman 2003). However, the growth of the central BH will consume a substantial fraction of the disk mass. The fraction of the disk mass that goes into stars rather than the BH is worthy of further investigation.

- *Binary BHs (BBHs) and coevolution of galaxies and QSOs/AGNs:* In the current coevolution model of galaxies and QSOs (Kauffmann & Haehnelt 2000), the nuclear activity of galaxies are triggered by major mergers of galaxies. Mergers of galaxies may form a BBH if there exists a massive BH in each of the merging galaxies (Begelman, Blandford & Rees 1980; Yu 2002; Volonteri, Haardt & Madau 2003). The evolution of the accretion disk around a massive BBH may be different from that around one BH (e.g., because of different boundary conditions) and depend on the orientation of the BBH orbital plane and BH spins. For example, studies of the time-dependent evolution of the accretion disk around the primary of a binary star with the outer disk radius tidally truncated by the secondary also yield self-similar solutions but with a steeper time dependence of the accretion rate $\dot{M}_d \propto \tau^{-2.5}$ (Thomson opacity) or $\tau^{-3.2}$ (Kramers opacity) (Lipunova & Shakura 2000; see also a different self-similar solution for an external disk around a binary star by Pringle 1991). The consistency of the slope of the accretion rate function with the expectation of our simple model may suggest that galaxy mergers have not been sufficiently efficient in faint AGNs to form a large population of BBHs, or that galaxy triaxiality or gas dynamics has caused BBHs to merge very quickly. It is worthwhile incorporating the evolution of BBHs and the evolution of accretion disks in models for the co-evolution of galaxies and QSOs/AGNs. One could then make joint predictions for the evolution of the QSO/AGN luminosity function as well as their accretion rate distribution function for comparison with observations.

- *Possible difference between AGNs and bright QSOs:* The luminosity evolution of bright QSOs ($L_{\rm bol} \gtrsim 10^{46}\,{\rm erg\,s^{-1}}$) is constrained from observations through a relation between the BH mass function in nearby normal galaxies and the time integral of the QSO luminosity function in Yu & Lu (2004a). The characteristic timescale for the luminosity of the QSO to decline during its second evolution phase was shown to be very short ($< 0.3\tau_{\rm Sp}$; Yu & Lu 2004a), significantly shorter than the timescale obtained for AGNs in this paper.[1] This difference between AGNs and bright QSOs is slightly smaller if we include Type I AGNs, but it still persists (see discussion at the end of § 3). In Yu & Lu (2004a), the luminosity in the second phase is assumed to decrease exponentially, and not according to a power-law. If the QSO luminosity evolution is assumed to have the same evolutionary form as described in equations (9) and (10), an even smaller τ_D (and/or larger γ) would be required. According to equation (16), τ_0 (or τ_D) is highly sensitive to the location of reservoir of accreting materials ($\propto R_0^{7/3}$) but depends weakly on $M_{\rm BH}$ and M_d. A smaller τ_D for QSOs implies that the disk size or the location of the material that fuels the BH in QSOs is not larger than in AGN; this is surprising because the BHs in QSOs are one or two orders of magnitude larger than the BHs of the AGNs that we have studied in this paper. This may provide interesting constraints on the fueling mechanisms that remove the angular momentum of materials at galactic scales and cause them to circularize at the parsec scale. A larger γ might suggest the existence of BBHs in QSOs (see also the discussion above).

- *Unified Models of AGNs: adding the effect of an evolving accretion disk* In current unified models of AGNs, orientation effects are proposed to explain the diversity of AGNs/QSOs (Antonucci 1993). The accretion rate and the Eddington ratio have also been proposed as important parameters for understanding why AGNs are so diverse (Boroson 2002). In this paper, we connect the diversity of the Eddington ratio in AGNs with the evolution of accretion disks, and we suggest different kinds of AGNs can be partly unified by considering the time sequence of the disk evolution.
  - *Lack of a torus in very weak AGNs:* The current AGN unification model requires the existence of a torus in an AGN, but observations show that it does not exist in M87 (Whysong & Antonucci 2004). Here we propose that the lack of a torus may be explained as an evolutionary consequence of the accretion process. At an early stage, the outer disk may be thick and clumpy and play the role of torus. At very late stage, most of the outer disk (or the torus) is very likely to have diffused away and the emission from the rest of the torus may be too weak to detect. M87 has a low Eddington ratio $\lesssim 10^{-3}$ (Di Matteo et al. 2003) and may correspond to the very late stage of the disk evolution in our scenario. Note that this diffusing torus scenario is different from the receding torus model in which luminous AGNs may have weak torii due to sublimation (Lawrence 1991). Generally, the evolution of a torus (or outer disk) will be driven by both diffusion and sublimation.
  - *Radiatively inefficient accretion:* With the decrease of the accretion rate in the second evolutionary phase (but before it decreases down to the Bondi accretion rate), the accretion may transit to a radiatively inefficient mode (ADAF or ADIOS; Narayan & Yi 1994; Blandford & Begelman 1999). The existence of some AGNs whose spectra need to be explained through radiatively inefficient accretion modes (but with an accretion rate large than the Bondi accretion rate) may thus also explained as a consequence of the evolutionary sequence described in this paper. The distribution of the normalized accretion rates of nearby low-luminosity AGNs could provide constraints on the

[1] The shortness of the characteristic timescale for QSOs can be explained as follows : (i) for a given BH mass, the peak nuclear luminosity decreases with increasing characteristic timescale (see eq. 11); (ii) because the local BH mass function decreases exponentially at the high-mass end, a long characteristic timescale results in QSO number densities that are much lower than the observed ones. Note that the characteristic timescale here is different from the "lifetime" of the nuclear activity phase. The value of the QSO lifetime is sensitive to the detailed definition of "nuclear activity"(e.g., the lower threshold of the nuclear luminosity for a galaxy to be classified as "active"). The determination of lifetime is more likely to be affected by uncertainties of the QSO luminosity function at the faint end. See more discussions in Yu & Lu (2004a).

transition from radiatively efficient accretion mode to the radiatively in-efficient mode (see also Begelman & Celotti 2004).

– *Radio-loud vs. radio-quiet:* AGNs/QSOs can be classified into two groups: radio-loud and radio quiet. It has been a long-standing question whether all AGNs pass through a radio-loud phase or whether only certain objects develop jets and become radio loud. Boroson (2002) shows that most radio-quiet QSOs have high Eddington-ratios, while most radio-loud QSOs have low ratios. Since the accretion rate decreases with time as the accretion disk evolves, we propose that from the evolutionary point of view, a QSO/AGN appears to be radio-quiet at its early evolution stage and appears radio-loud at its late stage (of course, the detailed appearance is also complicated by orientation effects and possibly BH spins).

6. Conclusions

In this paper we have connected the accretion rate distribution of nearby SDSS AGNs with the accretion physics around massive BHs. The observed distribution is consistent with a scenario in which the mass accretion rates in most nearby Seyfert galaxies are declining with time in a power-law form and the accretion process follows a self-similar evolutionary pattern as simple theoretical models predict. The results suggest that the observed diversity in the Eddington ratios of AGNs is a natural result of the long-term evolution of accretion disks. Some issues deserving of further investigation are discussed, such as on the long-term evolution of accretion disks (including self-gravitating disks), evolution of BBHs in QSOs/AGNs, coevolution of galaxies and QSOs/AGNs, and the unification picture of AGNs.

QY acknowledges support provided by NASA through Hubble Fellowship grant #HF-01169.01-A awarded by the Space Telescope Science Institute, which is operated by the Association of Universities for Research in Astronomy, Inc., for NASA, under contract NAS 5-26555.

REFERENCES

Antonucci, R. 1993, ARA&A, 31, 473

Begelman, M. C., Blandford, R. D., & Rees, M. J. 1980, Nature, 287, 307

Begelman, M. C., & Celotti, A. 2004, MNRAS, 352, 45

Blandford, R. D., & Begelman, M. C. 1999, MNRAS, 303, L1

Boroson, T. A. 2002, ApJ, 565, 78

Boyle, B. J., Shanks, T., Croom, S. M., Smith, R. J., Miller, L., Loaring, N., & Heymans, C. 2000, MNRAS, 317, 1014

Cannizzo, J. K., Lee, H. M., & Goodman, J. 1990, ApJ, 351, 38

Di Matteo, T., Allen, S. W., Fabian, A. C., Wilson, A. S., & Young, A. J. 2003, ApJ, 582, 133

Fabian, A. C. 2004, Carnegie Observatories Astrophysics Series, Vol. 1: Coevolution of Black Holes and Galaxies, ed. L. C. Ho (Cambridge: Cambridge Univ. Press)

Ferrarese, L., & Merritt, D. 2000, ApJ, 539, L9

Fromang, S., Balbus, S. A., & De Villiers, J.-P. 2004, ApJ, 616, 357

Gammie, C. F., Narayan, R., & Blandford, R. 1999, ApJ, 516, 177

Gebhardt, K., et al. 2000, ApJ, 539, L13

Goodman, J. 2003, MNRAS, 339, 937

Hao, L., et al. 2005, astro-ph/0501042, AJ, in press

Heckman, T. M., Kauffmann, G., Brinchmann, J., Charlot, S., Tremonti, C., & White, S. D. M. 2004, ApJ, 613, 109

Kaspi, S., Smith, P. S., Netzer, H., Maoz, D., Jannuzi, B. T., & Giveon, U. 2000, ApJ, 533, 631

Kauffmann, G., et al. 2003a, MNRAS, 341, 54

Kauffmann, G., et al. 2003b, MNRAS, 346, 1055

Kauffmann, G., & Haehnelt, M. 2000, MNRAS, 311, 576

Kondratko, P. T. Greenhill, L. J., & Moran J. M. 2005, ApJ, 618, 618

Lawrence, A. 1991, MNRAS, 252, 586

Lin, D. N. C., & Pringle, J. E. 1987, MNRAS, 225, 607

Lin, L., et al. 2004, ApJ, 617, L9

Lipunova, G. V., & Shakura, N. I. 2000, A&A, 356, 363

Lodato, G., & Bertin, G. 2003, A&A, 398, 517

Marconi, A., Risaliti, G., Gilli, R., Hunt, L. K., Maiolino, R., & Salvati, M. 2004, MNRAS, 351, 169

McLure, R. J., & Dunlop, J. S. 2004, MNRAS, 352, 1390

Miyoshi, M., Moran, J., Herrnstein, J., Greenhill, L., Nakai, N., Diamond, P., & Inoue, M. 1995, Nature, 373, 127

Narayan, R., & Yi, I. 1994, ApJ, 428, L13

Pringle, J. E. 1981, ARA&A, 19, 137

Pringle, J. E. 1991, MNRAS, 248, 754

Richstone, D., et al. 1998, Nature, 395, 14

Schmidt, M. 1968, ApJ, 151, 393

Schmidt, M., & Green, R. F. 1983, ApJ, 269, 352

Small, T. A., & Blandford, R. D. 1992, MNRAS, 259, 725

Tremaine, S., et al. 2002, ApJ, 574, 740

Volonteri, M., Haardt, F., & Madau, P. 2003, ApJ, 582, 559

Wandel, A., Peterson, B. M., & Malkan, M. A. 1999, ApJ, 526,579

Whysong, D., & Antonucci, R. 2004, ApJ, 602, 116

Woo, J.-H., & Urry, C. M. 2002, ApJ, 579, 530

Yu, Q. 2002, MNRAS, 331, 935

Yu, Q., & Lu, Y. 2004a, ApJ, 602, 603

Yu, Q., & Lu, Y. 2004b, ApJ, 610, 93

Yu, Q., & Tremaine, S. 2002, MNRAS, 335, 965

This preprint was prepared with the AAS LATEX macros v5.2.